

An Interactive Shader for Natural Diffraction Gratings

Bachelorarbeit

der Philosophisch-naturwissenschaftlichen Fakultät
der Universität Bern

vorgelegt von

Michael Single

2014

Leiter der Arbeit:
Prof. Dr. Matthias Zwicker
Institut für Informatik und angewandte Mathematik

Abstract

In nature, color production is the result of physical interaction of light with a surface's nano-structure. In his pioneering work, Stam developed limited reflection models based on wave optics, capturing the effect of diffraction on very regular surface structures. We propose an adaption of his BRDF model that can handle complex natural gratings. On top of this, we describe a technique for interactively rendering diffraction effects, as a result of physical interaction of light with biological nano-structures such as snake skin. As input data, our method uses discrete height fields of natural gratings acquired by using atomic force microscopy (AFM). Based on Taylor Series approximation, we leverages precomputation to achieve interactive rendering performance (about 5-15 fps). We demonstrate results of our approach using surface nano-structures of different snake species applied on a measured snake geometry. Lastly, we evaluate the quality of our method by a comparison of the maxima for peak viewing angles using the data produced by our method against the maxima of the grating equation.

Contents

1 Results	1
1.1 BRDF maps	1
1.2 Rendering Surface Geometries	12
List of Tables	19
List of Figures	19
List of Algorithms	20
Bibliography	21

Chapter 1

Results

In this chapter we examine the rendered output results of our implementation of our BRDF models applied to different input patches such as Blaze grating or Elaphe ?? and Xenopeltis ?? snake nano-scaled surface sheds. We are discussing and comparing both, their BRDF maps 1.1 and the corresponding renderings on a snake geometry like shown in section 1.2 for various input parameters. Last we also show a real experimental image showing the effect of diffraction for similar parameters like we have.

1.1 BRDF maps

A BRDF map shows a shader's output for all possible viewing directions for a given, fixed, incident light direction. We assume that each viewing direction is expressed in spherical coordinates (See appendix ??) (θ_v, ϕ_v) and is represented in the map at point

$$(x, y) = (\sin(\theta_v)\cos(\phi_v), \sin(\theta_v)\sin(\phi_v)) \quad (1.1)$$

with its origin at the map center. The light direction for normal incidence (θ_i, ϕ_i) has been fixed to $(0, 0)$ for our rendered results.

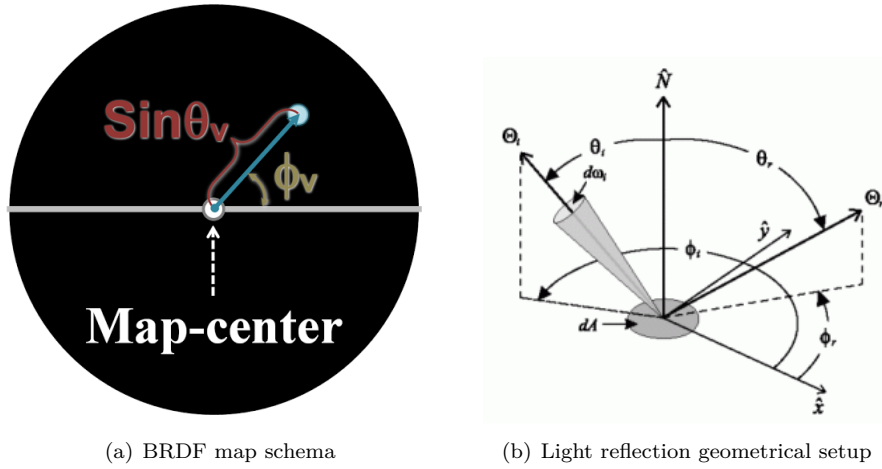


Figure 1.1: BRDF maps¹ for different patches: $\Theta = (\theta_i, \phi_i)$ is the direction of light propagation

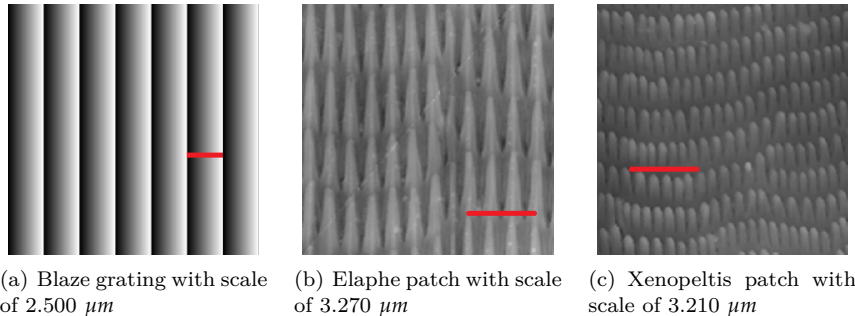


Figure 1.2: Cutouts of our nano-scaled surface gratings used for rendering within our shader with a scale indicator (red line) for each patch. Note that for rendering, we use larger patches.

Figure 1.3 shows the BRDF maps of the full lambda space sampling approach (**FLSS** like introduced in section ??) as described in section ?? applied on different nanoscale surface gratings as shown in figure 1.2. In Subfigure 1.3(a) we see the BRDF map for the Blazed grating, showing high relative brightness for its first order diffraction, i.e. for the Blazed gratings most of the diffracted spectral energy lies in its first order. Notice that the surface of blazed grating is forming a step structure for which the angle between the step normal and the grating normal is denoted by *blaze angle*. Every blazed grating is manufactured in the Littrow² configuration. This means that the blaze angle is chosen such that the diffraction angle and incidence angle are identical. Thus it a blazed grating it has a maximal efficiency for the wavelength of the used light. Higher diffraction modes are still perceivable (second and higher diffraction orders) but with a much lower relative

¹image source of figure:

- 1.1(a): Taken from D.S.Dhillon's Paper [D.S14]
- 1.1(b): Taken from <http://math.nist.gov/~FHunt/appearance/brdf.html>

²For further information please see http://en.wikipedia.org/wiki/Blazed_grating.

brightness. The asymmetry of the pattern is due to the asymmetric geometry of the grating 1.2(a).

The finger-like structures contained in the Elaphe surface grating 1.2(b) are quite regularly aligned and hence diffraction occurs along the horizontal axis for the BRDF map as shown in figure 1.3(b). The reason for not seeing any strong diffraction color contribution along other directions in the BRDF map is due to the fact that these ‘nano-fingers’ overlap across layers and thus do not exhibit any well-formed periodicity along finger direction.

For Xenopeltis surface grating 1.2(c), we observe diffraction along many different, almost vertical directions in the BRDF map 1.3(c) since the layers of the finger-like structures do not overlap and are shifted significantly along their length but still exhibit some local consistency. A similar argument holds true for diffraction across locally periodic finger patches with slightly different orientations.

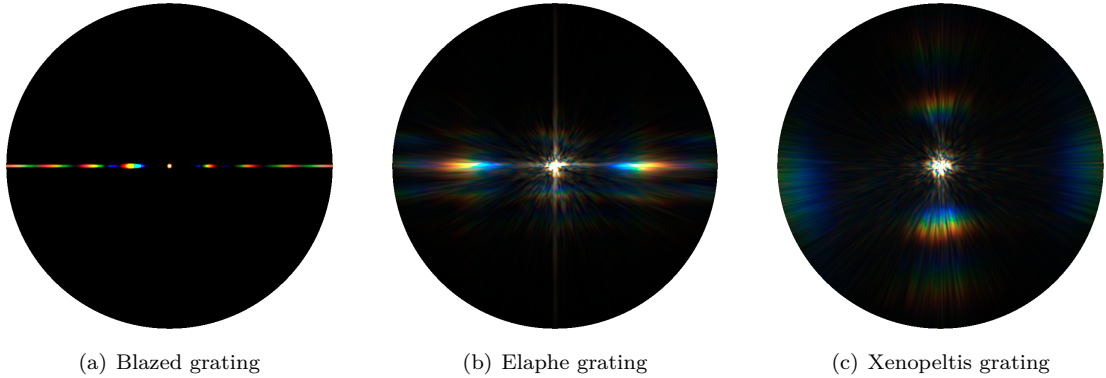


Figure 1.3: BRDF maps for different patches

Figure 1.4 shows BRDF maps of all our BRDF models applied on the Blaze grating. Figure 1.4(a) shows the FLSS shading approach result for our blazed grating and it is used in order to compare with our other rendering approaches.

Figure 1.4(b) shows the BRDF map for the NMM approach, introduced in section ??, which is close to the FLSS approach, verified in section ??, just like in the case of corresponding evaluation in figure ???. Nevertheless there is a small, noticeable difference: For the NMM approach we see a white, circular spot around the map center. Nevertheless, apart from this white spot, the NMM approach resembles the FLSS approach. The reason for this differences is due to the fact that the NMM approach treats the center of a BRDF map as a special case, like described in section ???. Technically, every location around a small ϵ -circumference from the map center gets white color assigned.

Figure 1.4(c) shows the BRDF map for the PQ approach which relies on sinc-interpolation. The PQ BRDF map and the FLSS results are visual alike. Compared to the evaluation plots in figure ???, the BRDF maps even persuade more. Compared to FLSS, one difference we notice is that the first order of diffraction is a little spread for the PQ approach. Without³ applying a sinc-interpolation, this spreading effect would be even strengthened.

³Note that if we do not perform a sinc-interpolation this would correspond to apply a linear interpolation instead.

Last, let us consider figure 1.4(d) which shows the BRDF map produced by using Nvidia Gem's implementation [JG04] of Stam's BRDF model when constraining the y-axis of the BRDF map. This corresponds to a 1d diffraction grating, along the x-axis. This model only uses the spacing d of a given grating. It also always produces highly symmetric results.

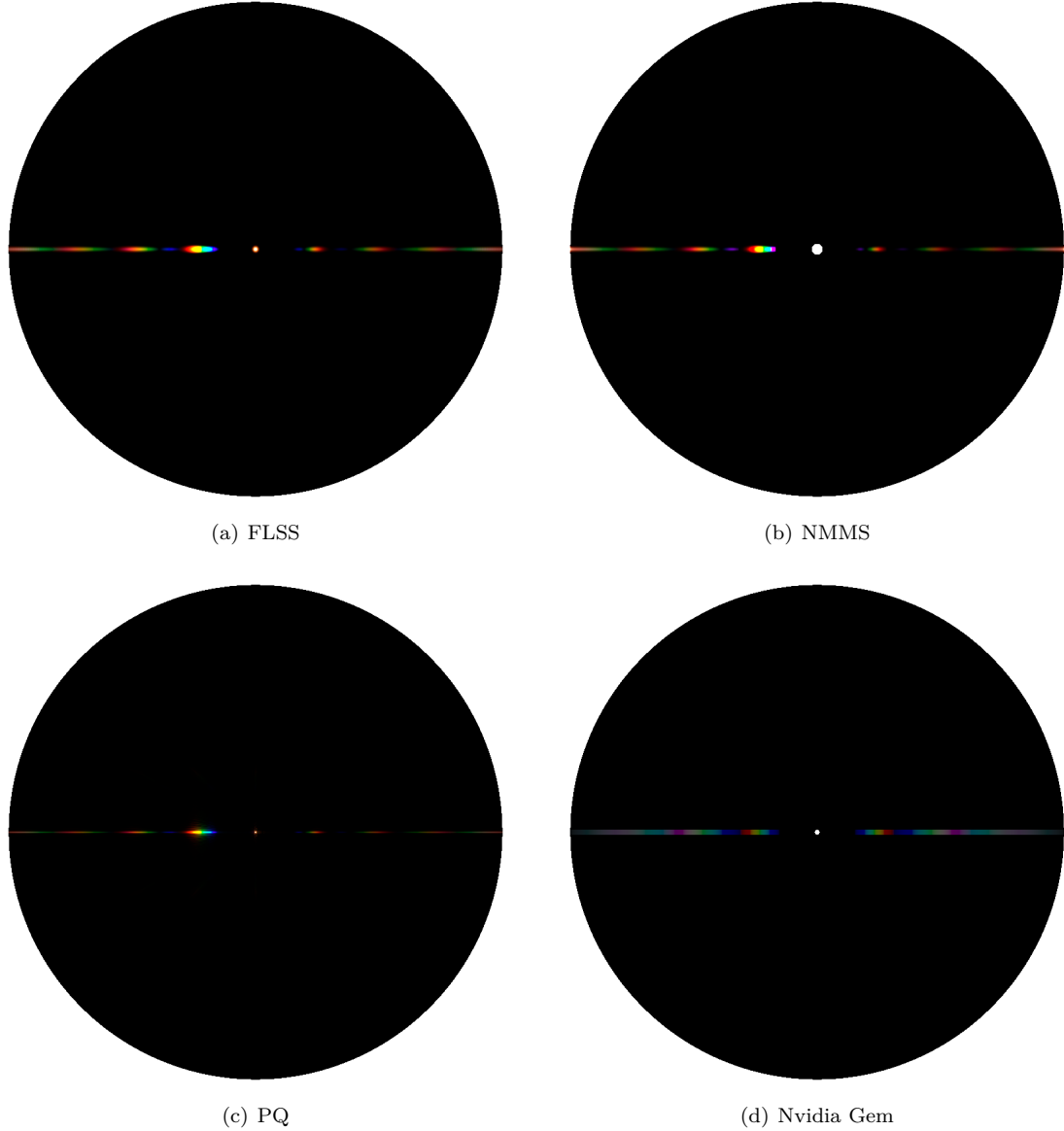


Figure 1.4: BRDF maps for Blazed grating comparing our different rendering approaches

Figure 1.5 and figure 1.6 show the BRDF maps for different wavelength step sizes used in the fragment shader for the FLSS approach applied on the blazed grating and the Elpahe snake shed, respectively. Within our fragment shaders the outermost loop iterates over the range $[380nm, 780nm]$

for a given step size λ_{step} to integrate over the wavelength spectrum. Having bigger step sizes implies having fewer λ -samples which will reduce the overall runtime of a shader but, it will also introduce artifacts and therefore lower the overall shading quality. For Elaphe surface grating, artifacts are perceivable when $\lambda_{step} \leq 10nm$. Results produced by using $5nm$ step sizes do not differ from those produced by using $\lambda_{step} = 1nm$. This allows us to set λ_{step} at $5nm$. For a Blazed grating we may chose even bigger step sized without losing any rendering quality(see figure 1.5).

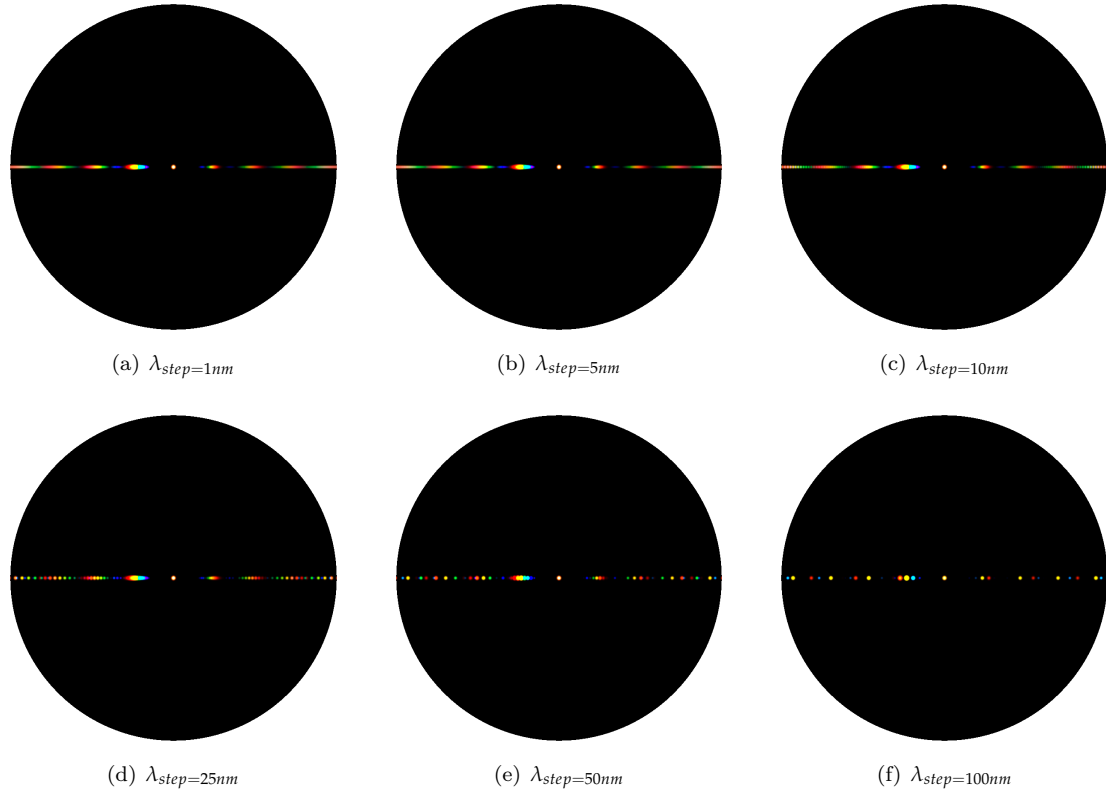
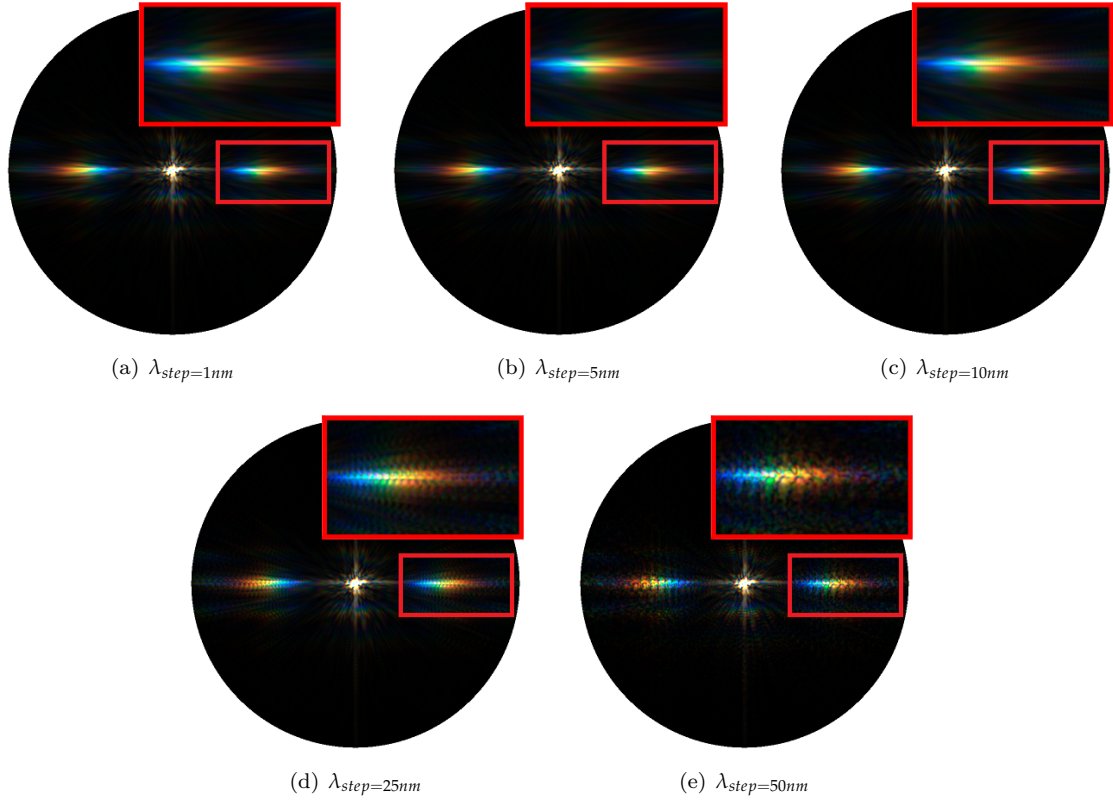


Figure 1.5: Blazed grating at $2.5\mu m$: Different λ step sizes

Figure 1.6: Elaphe grating at $65\mu m$: Different λ step sizes

The figures 1.7, 1.8, 1.9 show a comparison of the BRDF maps produced by the FLSS approach (on the left) and the PQ shading approach (on the right) applied on all our patches. For Blazed grating, as already mentioned, we notice that both approaches, FLSS and PQ, resemble each other. We also notice that for PQ map, the first order diffraction color contribution is spread. For the Elaphe and Xenopeltis grating we notice similar shaped BRDF patterns, even when the angle of light varies, but nevertheless, they also contain some artifacts.

In general, a Blazed Grating is manufactured in a way that a large fraction of the incident light is diffracted preferentially into the first order. Therefore, most of the energy in its BRDF map lies in the first order of diffraction at its blaze angle. This implies that largest portion of the color contribution, visible on the corresponding BRDF map, lies at that angle. In figure 1.7, in contrast to the results produced by the FLSS approach, we see color fringes at the first order modes in the BRDF map produced by our PQ approach. This implies that the PQ approach does not produce reliable results which also affirms our evaluation plots shown in figure ???. A similar argumentation hold true for the PQ approach, when we do not apply we a sinc-interpolation like shown in figure 1.7(c).

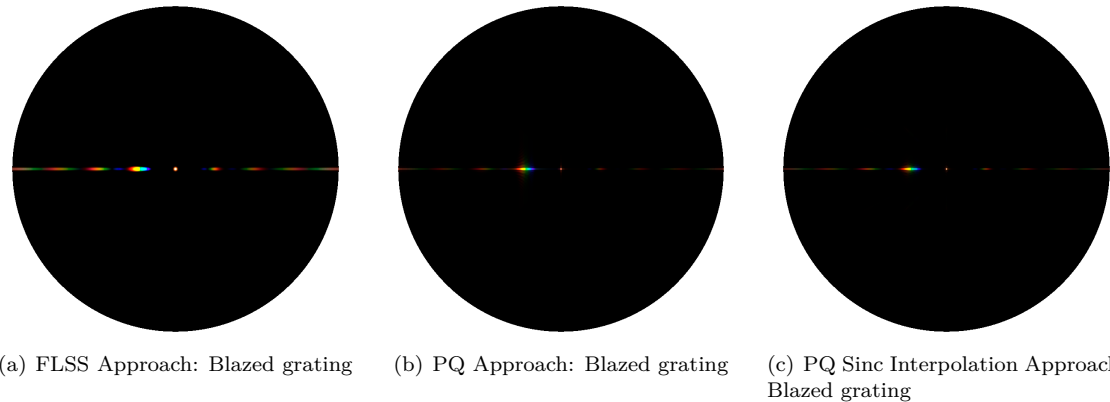


Figure 1.7: A comparison between the PQ- and the FLSS approach applied on an Blazed grating.

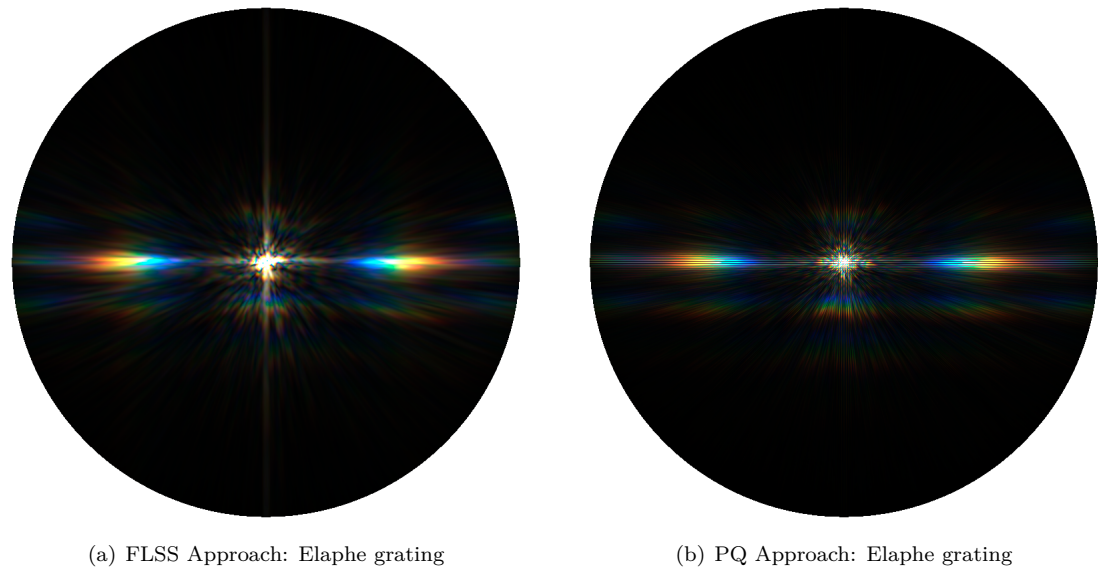


Figure 1.8: A comparison between the PQ- and the FLSS approach applied on an Elaphe grating.

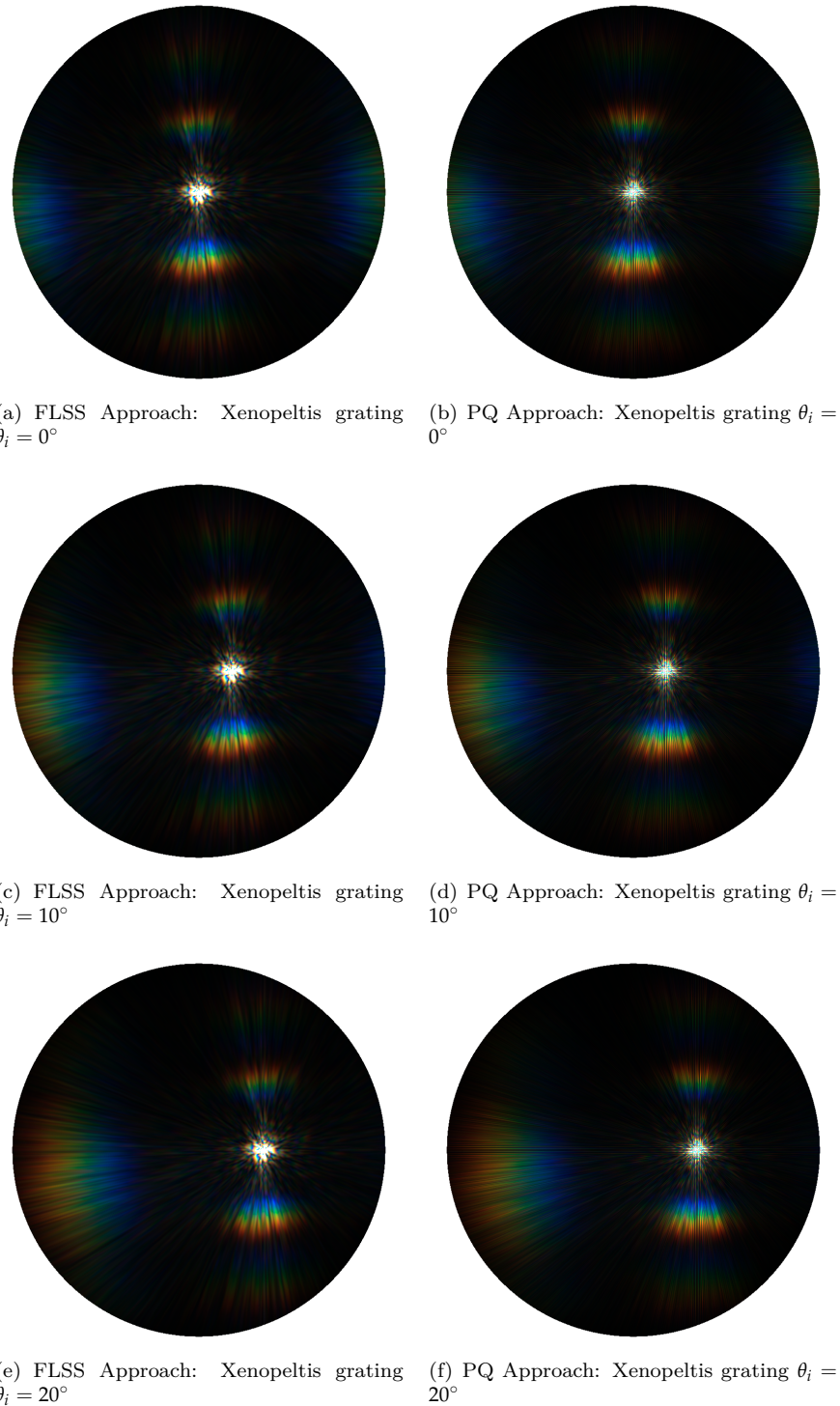


Figure 1.9: A comparison between the PQ- and the FLSS approach applied on an Xenopeltis grating.

Figure 1.10 shows BRDF maps for the full lambda sampling approach applied to the Blazed grating, while varying the value for the spatial variance σ_s . This akin to changing the coherence length for the incident light. The lower the coherence length, the fewer interacting grating periods produce blurred diffraction bands for different λ which overlap to produce poorly resolved colors.

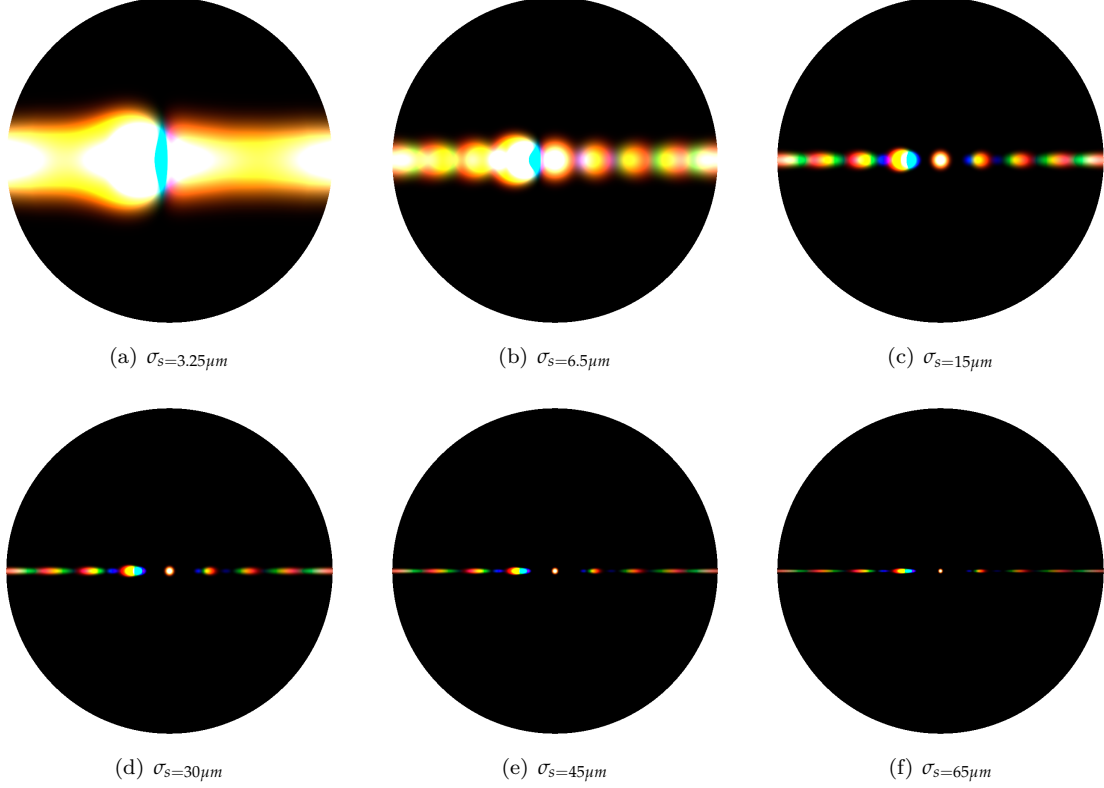


Figure 1.10: Blazed grating with periodicity of $2.5\mu m$: Different σ_s

Figures 1.11 and 1.12 show the BRDF maps the reference-, FLSS approach using different values for N in the taylor series approximation. For both input patches we clearly visually observe the convergence of the taylor series for higher values of N . We visually observe convergence of the Taylor series for all our patches a very large value of N^4 .

Like discussed in section ?? there exists a certain value of N for which our approach converges. For all our shading approaches, applied on our gratings, we visually observed a convergence of their BRDF maps when using $N \geq 39$ DFT terms. Furthermore, for a Blazed grating it satisfies to use only $N \geq 7$ - and for an Elaphe grating only $N \geq 9$ DFT terms. Notice, that these numbers of required DFT terms were empirically determined by trial and error strategy.

However, by making use of taylor error term estimates, like introduced in the appendix section ??, we can derive an upper bound for N . Since this computation is dependent on many aspects, such as on the grating spacing, the pixel-width correspondence, the used lambda space for sam-

⁴Using N equal to 39 lead to visual convergence for all our used gratings.

pling, it is usually simpler to determine empirically actual values for N .

In algorithm ?? we compute the DFT terms of a provided height field h raised to the power of the imaginary number i times an integer, i.e. we evaluate the expression $DFT(h)^n \cdot i^n$. Since we multiply our height field by i^n and then apply the DFT operator, basically, there exist four possible convergence images, each having its own convergence radius.

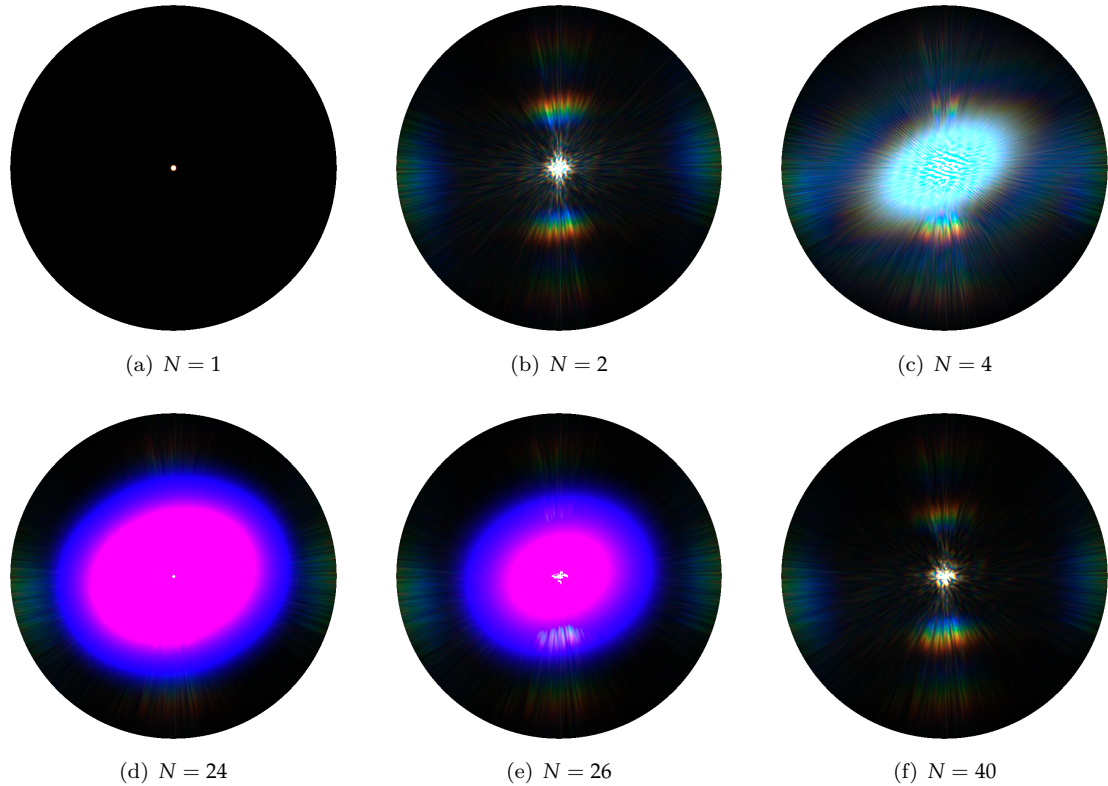


Figure 1.11: Blazed grating at $65\mu m$: N Taylor Iterations

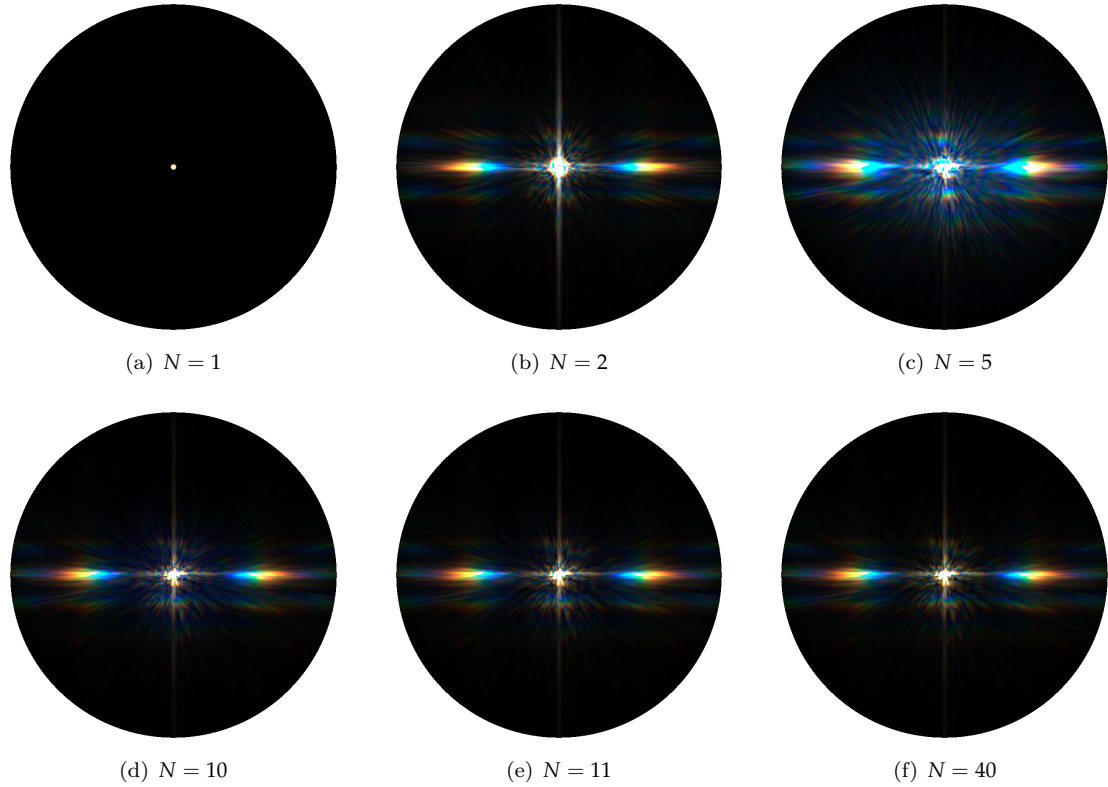
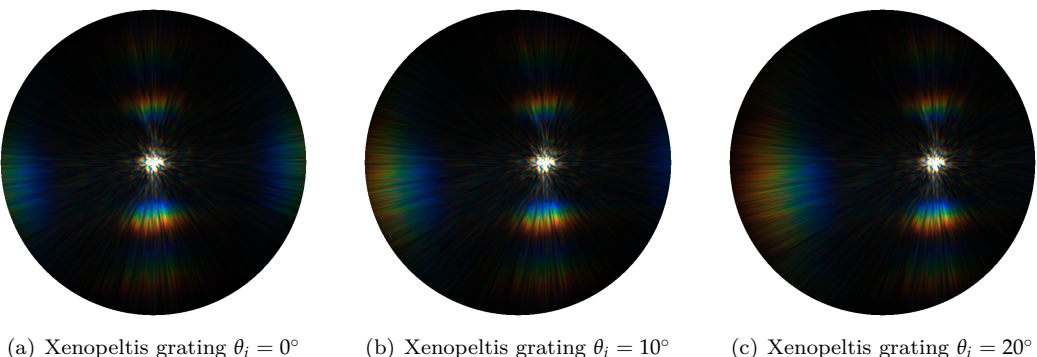
Figure 1.12: Elaphe grating at $65\mu m$: N Taylor Iterations

Figure 1.13 shows the BRDF maps of the FLSS approach applied on the Xenopeltis snake shed, using different θ_i incident angles. When slightly moving the incident angle θ_i , we can observe how the BRDF map changes. For higher values of θ_i we start seeing diffraction color contribution on the right side of the BRDF map.

Figure 1.13: BRDF maps for Xenopeltis grating: different θ_i angles

1.2 Rendering Surface Geometries

In this section we are going to present our actual renderings simulating the effect of diffraction caused when a directional light source encounters different nano-scaled surfaces on a given curved snake mesh. We will see that diffraction colors change dramatically with changes in light direction, surface normals and viewing direction, which is typical for diffraction colors observed in nature. For rendering we are going to rely on our FLSS approach. Unfortunately, this approach is rather slow and can barely be considered as being interactively performing. Nevertheless, we have introduced some optimizations in order to make it interactive.

All rendered results shown in this section are produced by the FLSS approach since we have proven its validity in figure ???. Therefore, we can trust its renderings and may consider them as being accurate. Furthermore, as support of our evaluation plots regarding the NMM approach, that are shown in figure ???, we also show results produced by the NMM approach.

The Laboratory of Artificial and Natural Evolution in Geneva provided us by a triangular mesh of a snake. This mesh was produced by a 3d scan of a Elaphe snake species and consists of 11696 vertices and 22950 faces. Note that, for all our renderings, we used this snake mesh.

Among all the snake species under consideration, their macroscopic geometry is highly similar. Only the geometry of their nano-structures varies and is responsible for a snake's iridescence. Thus, we can use the same snake surface model to render diffraction for different species. Table 1.1 lists the system specifications of the machine I used in order to produce the rendered images.

Processor	Intel i7 CPU 970 @ 3.20 GHz (12 CPUs)
Memory	12288 MB RAM
Graphics Card	GeForce GTX 770
Graphics Clock	1150 MHz
Graphics Memory	4096 MB
Graphics Memory Bandwidth	230.4 GB/s MHz

Table 1.1: Hardware specifications of the machine used to render snake surface. Statistics are provided using the tool *NVIDIA Geforce Experience*.

Figure 1.14 shows renderings produced by the FLSS approach applied on our snake mesh for different, given input patches. Due do the fact that a Blazed grating has its maximum intensity for a certain direction and the geometry of the snake mesh is curved i.e. is non-flat, we can expect rather less diffraction color contribution like shown in figure 1.14(b).

In contrast, For both the renderings, we see colorful patterns on the skin of our snake species, Elaphe and Xenopeltis, due to the effect of diffraction. We see much less colorful patterns for Elaphe like shown in figure 1.14(b) than for Xenopeltis like shown in figure 1.14(c). This is consistent with the observations in the real world as shown in figure ???. As observable figure 1.2(b), the substructures (the finger like structures) in the height field of a Elaphe snake skin are not very regularly aligned along the y-axis. This is why the Elaphe species is less iridescent than the other specie. The Xenopeltis snake has a brownish body with no pigmentation, which makes the iridescence more spectacular than on Elaphe.

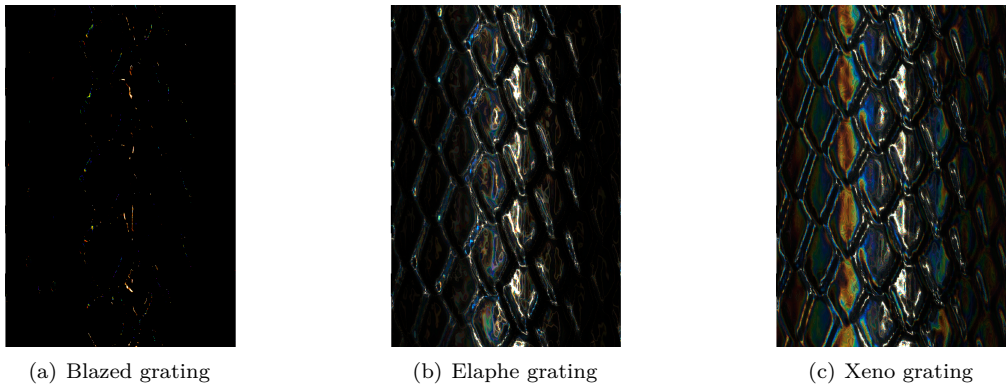


Figure 1.14: Diffraction of different snake skin gratings rendered on a snake geometry

Figure 1.15 shows a set of subfigures for rendering the effect of diffraction produced by the FLSS approach (used as our reference approach), applied on our snake mesh using the Elaphe nano structure. Figure 1.15(b) shows the final diffraction color contribution result with texture-blending. We only see little diffraction color contribution in this subfigure which resembles quite well to the reality as shown in figure ???. In subfigure 1.15(d) we see the light cone in order to show the direction of the light source besides the rendered results. Subfigure 1.15(e) is a sample Fourier image of Elpahe's nano-scale surface structure 1.15(d).

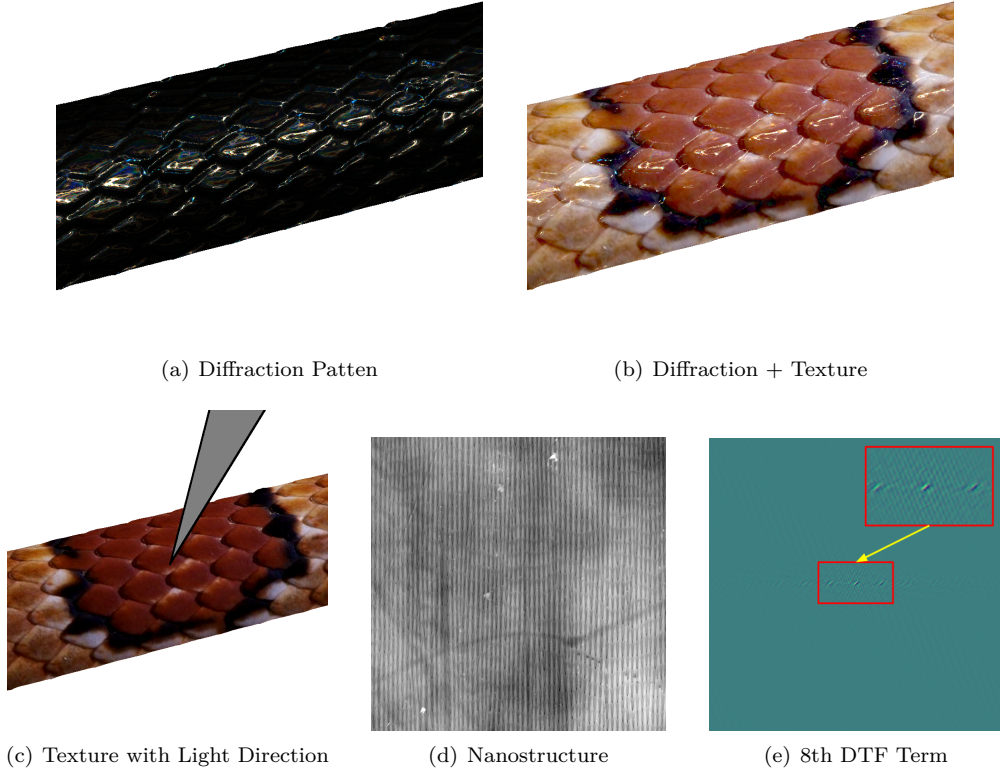


Figure 1.15: Diffraction for Elaphe snake skin produced by our reference approach.

Figure 1.16 shows a set of subfigures for the effect of diffraction for the Xenopeltis snake surface. For Xenopeltis we see quite a lot color contribution due the phenomenon of diffraction like shown in figure ???. Comparing this to a real image ?? we notice much resemblance regarding the reflectance strength and colorful pattern.

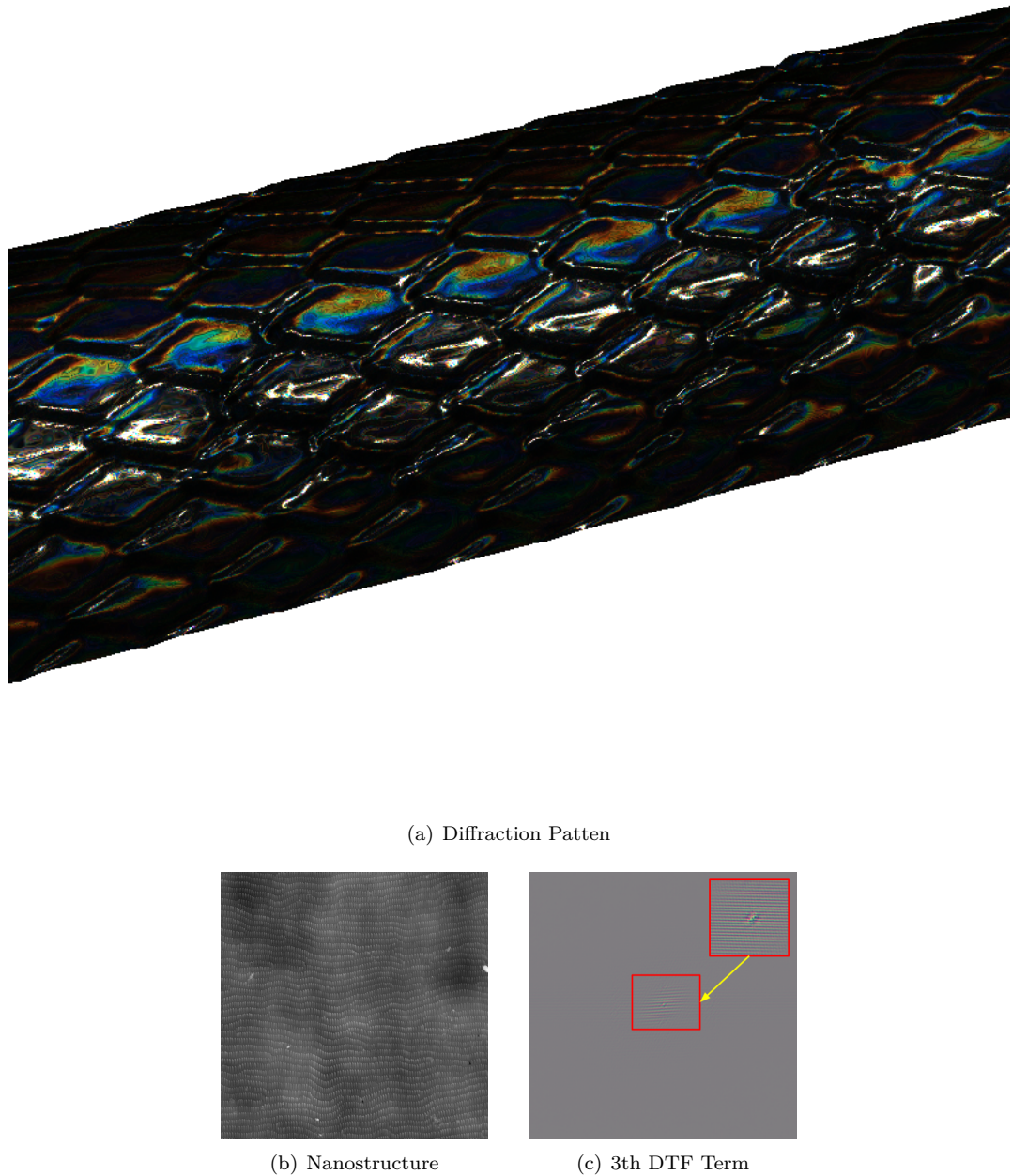


Figure 1.16: Diffraction for Xenopeltis snake skin produced by our reference approach.

Figure 1.17 shows the diffraction pattern for Elaphe snake shed at different zoom levels for fixed incident light and viewing direction. We changed the zoom-levels by adjusting the field of view angle of our camera. For each image in this figure, the one to its right side is a five times zoomed-in version of the region within its red box. The close up perspectives exhibit complex and colorful diffraction patterns.

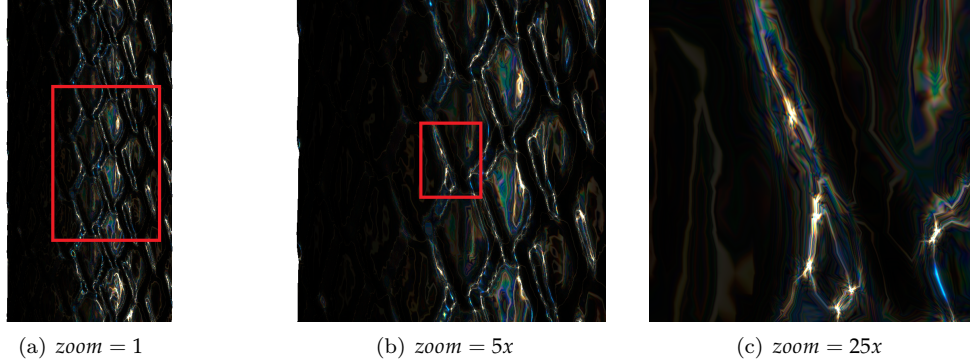


Figure 1.17: Diffraction on Elaphe snake skin grating: Different camera zoom levels by varying the field of view.

Figure 1.18 shows how the diffraction pattern changes when the incident light direction is moved slightly. This Figure gives us an impression what kind of complex, perspective-dependent pattern the diffraction phenomenon produces.

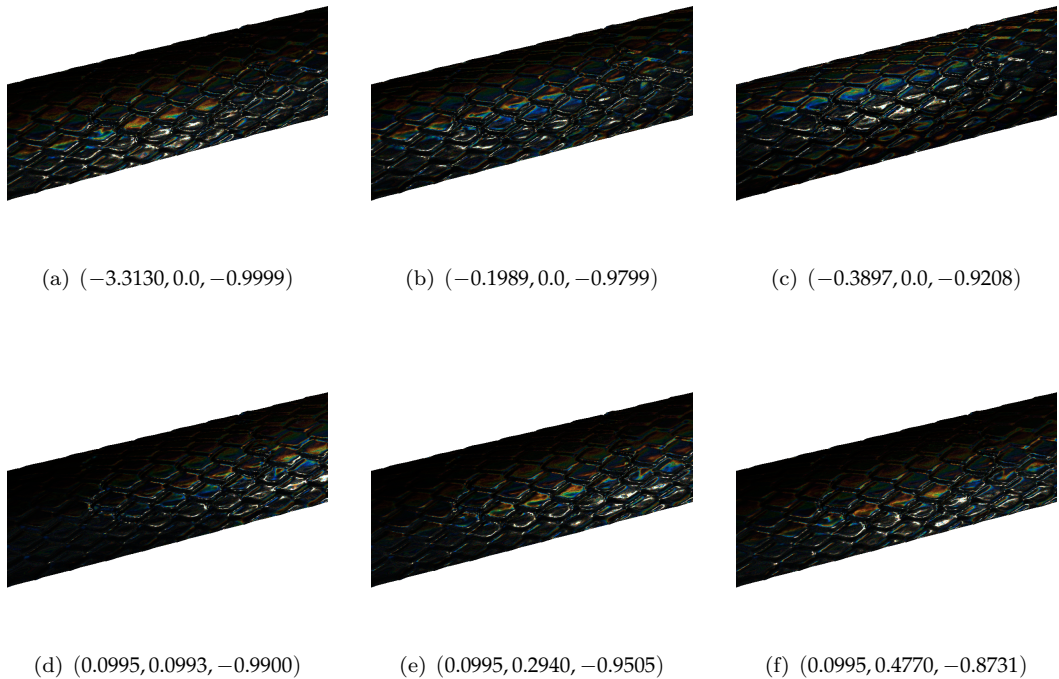


Figure 1.18: Diffraction on Elaphe snake skin grating: Different light directions

Figure 1.19 shows a photo of an experimental setup for demonstrating the effect of diffraction using a Elaphe snake grating. The exact parameters for the experimental setup are unknown. Nevertheless this image gives us an impression of how close our model is to the reality comparing it with our simulated results since we notice similar diffraction patterns for our simulated results using an Elaphe snake shed.

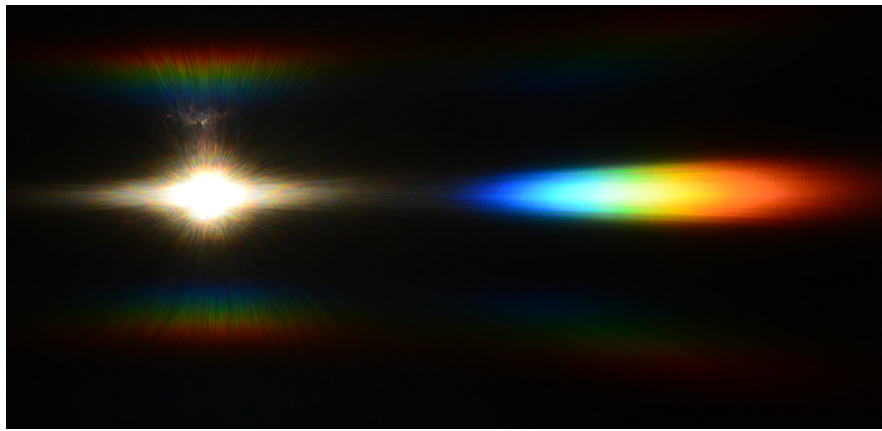
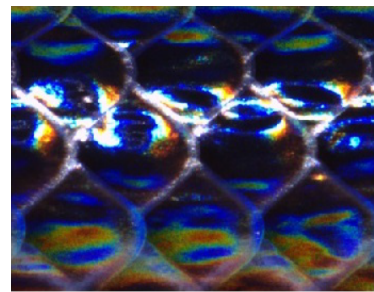
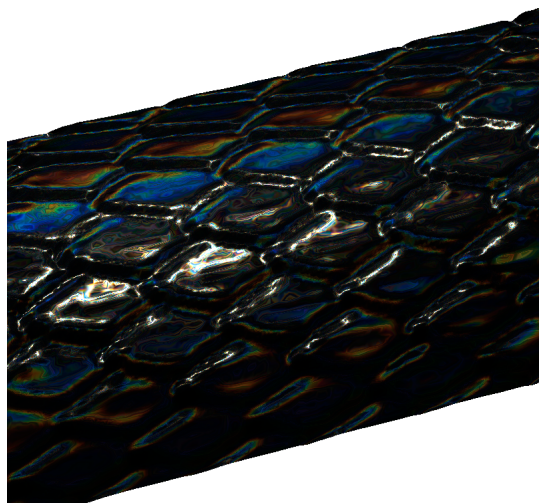


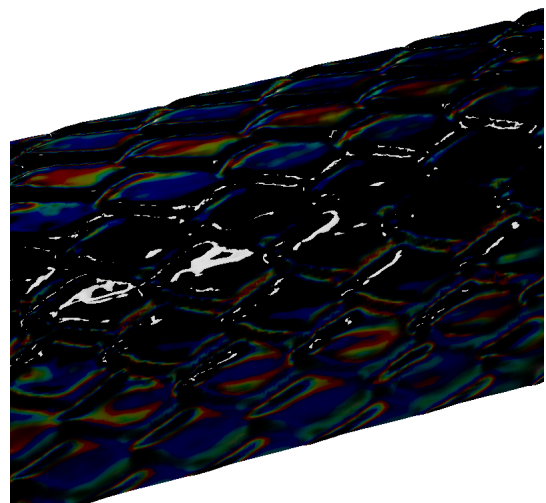
Figure 1.19: Diffraction Elaphe: experimental setup



(a) Xenopeltis Image



(b) FLSS



(c) Stam

Figure 1.20: Attempt to reproduce a real world image: FLSS- vs Stam’s Approach

List of Tables

1.1	Hardware Specifications	12
-----	-------------------------	----

List of Figures

1.1	BRDF Map	2
1.2	Our Diffraction Gratings	2
1.3	BRDF Map: FLSS Approach applied on various Gratings	3
1.4	BRDF Map: Our Approaches applied on a Blazed Grating	4
1.5	BRDF Map: Varying step sizes FLSS Blazed Grating	5
1.6	BRDF Map: Varying step sizes FLSS Elaphe Grating	6
1.7	BRDF Map: PQ vs FLSS Approach on Blazed Grating	7
1.8	BRDF Map: PQ vs FLSS Approach on Elaphe Grating	7
1.9	BRDF Map: PQ vs FLSS Approach on Xenopeltis Grating	8
1.10	BRDF Map: Different spatial variance σ_s values	9
1.11	BRDF Map: Xenopeltis Grating Convergence	10
1.12	BRDF Map: Elaphe Grating Convergence	11
1.13	BRDF Map: Varying Viewing Angles	11
1.14	Snake Renderings: Our Approaches applied on our Gratings	13
1.15	Snake Renderings: FLSS Approach for Elaphe Grating	14
1.16	Snake Renderings: FLSS Approach for Xenopeltis Grating	15
1.17	Snake Renderings: FLSS Approach for a varying FoV	16
1.18	Snake Renderings: FLSS Approach for varying Light Directions	17
1.19	Diffraction Elaphe: experimental setup	17
1.20	Snake Renderings: Stam's- vs. Flss- Approach on Xenopeltis	18

List of Algorithms

Bibliography

- [Bar07] BARTSCH, Hans-Jochen: *Taschenbuch Mathematischer Formeln*. 21th edition. HASNER, 2007. – ISBN 978-3-8348-1232-2
- [CT12] CUYPERS T., et a.: Reflectance Model for Diffraction. In: *ACM Trans. Graph.* 31, 5 (2012), September
- [DD14] D.S. DHILLON, et a.: Interactive Diffraction from Biological Nanostructures. In: *EUROGRAPHICS 2014/ M. Paulin and C. Dachsbacher* (2014), January
- [D.S14] D.S.DHILLON, M.Single I.Gaponenko M.C. Milinkovitch M. J.Teyssier: Interactive Diffraction from Biological Nanostructures. In: *Submitted at Computer Graphics Forum* (2014)
- [For11] FORSTER, Otto: *Analysis 3*. 6th edition. VIEWEG+TEUBNER, 2011. – ISBN 978-3-8348-1232-2
- [I.N14] I.NEWTON: *Opticks, reprinted*. CreateSpace Independent Publishing Platform, 2014. – ISBN 978-1499151312
- [JG04] JUAN GUARDADO, NVIDIA: Simulating Diffraction. In: *GPU Gems* (2004). <https://developer.nvidia.com/content/gpu-gems-chapter-8-simulating-diffraction>
- [LM95] LEONARD MANDEL, Emil W.: *Optical Coherence and Quantum Optics*. Cambridge University Press, 1995. – ISBN 978-0521417112
- [MT10] MATIN T.R., et a.: Correlating Nanostructures with Function: Structurnal Colors on the Wings of a Malaysian Bee. (2010), August
- [PAT09] PAUL A. TIPLER, Gene M.: *Physik für Wissenschaftler und Ingenieure*. 6th edition. Spektrum Verlag, 2009. – ISBN 978-3-8274-1945-3
- [PS09] P. SHIRLEY, S. M.: *Fundamentals of Computer Graphics*. 3rd edition. A K Peters, Ltd, 2009. – ISBN 978-1-56881-469-8
- [R.H12] R.HOOKE: *Micrographia, reprinted*. CreateSpace Independent Publishing Platform, 2012. – ISBN 978-1470079031
- [RW11] R. WRIGHT, et a.: *OpenGL SuperBible*. 5th edition. Addison-Wesley, 2011. – ISBN 978-0-32-171261-5
- [Sta99] STAM, J.: Diffraction Shaders. In: *SIGGRPAH 99 Conference Proceedings* (1999), August
- [T.Y07] T.YOUNG: *A course of lectures on natural philosophy and the mechanical arts Volume 1 and 2*. Johnson, 1807, 1807